ACS MATERIALS Au
AN OPEN ACCESS JOURNAL OF THE AMERICAN CHEMICAL SOCIETY

pubs.acs.org/materialsau Article

Single-Crystalline Germanium Nanocrystals via a Two-Step Microwave-Assisted Colloidal Synthesis from GeI_4

Zheng Ju, Xiao Qi,[§] Roy Sfadia,[§] Minyuan Wang, Emily Tseng, Elizabeth C. Panchul, Sue A. Carter, and Susan M. Kauzlarich*

Cite This: *ACS Mater. Au* 2022, 2, 330−342 Read Online

ACCESS | Metrics & More | Article Recommendations | Supporting Information

ABSTRACT: Colloidal germanium (Ge) nanocrystals (NCs) are of great interest with possible applications for photovoltaics and near-IR detectors. In many examples of colloidal reactions, Ge(II) precursors are employed, and NCs of diameter ∼3−10 nm have been prepared. Herein, we employed a two-step microwave-assisted reduction of GeI_4 in oleylamine (OAm) to prepare monodispersed Ge NCs with a size of 18.9 ± 1.84 nm. More importantly, the as-synthesized Ge NCs showed high crystallinity with single-crystal nature as indicated by powder X-ray diffraction, selected area electron diffraction, and high-resolution transmission electron microscopy. The Tauc plot derived from photothermal deflection spectroscopy measurement on Ge NCs thin films shows a decreased bandgap of the Ge NCs obtained from GeI_4 compared with that of the Ge NCs from GeI_2 with a similar particle size, indicating a higher crystallinity of the samples prepared with the two-step reaction from GeI_4. The calculated Urbach energy indicates less disorder in the larger NCs. This disorder might correlate with the fraction of surface states associated with decreased particle size or with the increased molar ratio of ligands to germanium. Solutions involved in this two-step reaction were investigated with ^{1}H NMR spectroscopy and high-resolution mass spectrometry (MS). One possible reaction pathway is proposed to unveil the details of the reaction involving GeI_4 and OAm. Overall, this two-step synthesis produces high-quality Ge NCs and provides new insight on nanoparticle synthesis of covalently bonding semiconductors.

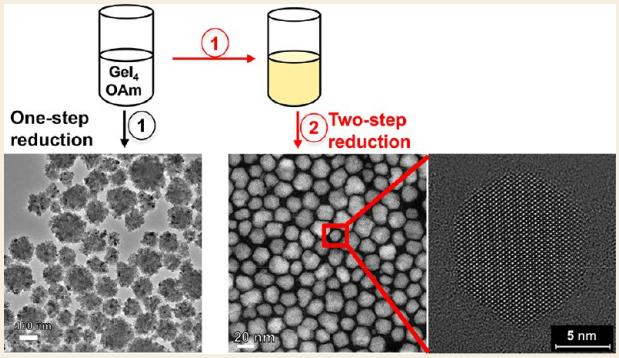

KEYWORDS: *Ge nanocrystals, microwave synthesis, single crystal, size control, photothermal deflection spectroscopy (PDS), Urbach energy*

1. INTRODUCTION

Ge, with its narrow bulk bandgap of 0.67 eV, can be tuned with the quantum confinement effect by controlling the particle size, which has been investigated broadly over decades.[1−3] High carrier mobilities as well as a large absorption coefficient and exciton Bohr radius (∼24 nm) make nanostructured Ge a promising candidate for solar energy conversion,[4−7] optoelectronics,[10−12] and bioimaging[13] as well as an anode material in lithium batteries.[8,9]

Colloidal methods have been developed for the synthesis of Ge NCs in the past decades. However, a solution-based method with precise control on the Ge NC size and morphology is still a challenge compared with noble metal nanocrystals and Cd- and Pd-based semiconductors because of the high crystallization temperature required for the formation of diamond-structured Ge.[12,14,15] As a result, some of the solution routes reported to date produce amorphous particles or particles with amorphous surfaces that are easily oxidized.[2,16] To avoid amorphous products, highly reactive reducing agents such as $LiAlH_4$, $NaBH_4$, hydrazine, and *n*-BuLi can be employed to produce crystalline Ge NPs.[12,17−20] The disadvantage of using strong reducing agents is a loss of the ease of synthesis and, for those employing a hydride reagent, toxic byproducts.

Ge NCs have been successfully prepared from GeI_2 via a microwave-assisted route that has been shown to be a highly reproducible method for preparing Ge particles.[2,21,22] While size control by employing the mixed halides, GeI_2 and GeI_4, or GeI_2 and halogens has been demonstrated,[3,21,22] the microwave-assisted synthesis of Ge NCs directly from Ge(IV) halides as the single source has not been reported to date. This is largely due to the different reduction potential of Ge(II) compared with Ge(IV). The reduction potential of Ge (II) to Ge(0) is +0.247 V and is easily reduced under mild conditions. On the other hand, the reduction potential of Ge(IV) to Ge(0)

Received: November 17, 2021
Revised: January 25, 2022
Accepted: January 25, 2022
Published: February 8, 2022

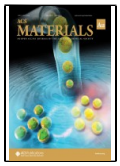

https://doi.org/10.1021/acsmaterialsau.1c00072
ACS Mater. Au 2022, 2, 330−342

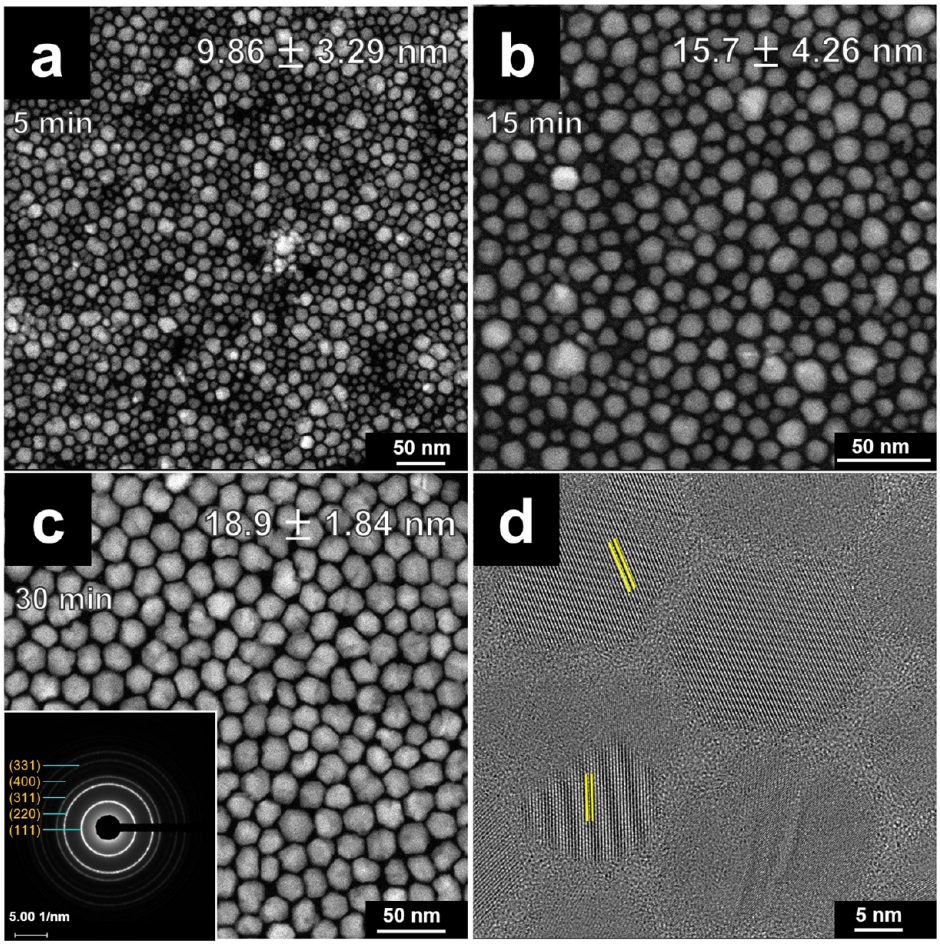

Figure 1. HAADF-STEM images of two-step reactions stopped at different times at the second step: (a) 5 min, (b) 15 min, and (c) 30 min. Inset of (c) is the SAED image of Ge NCs; sharp diffractions are assigned to the cubic Ge phase. (d) HRTEM image of the 30 min reaction shows high crystallinity and the single-crystal nature of as-synthesized Ge NCs; yellow lines indicate the (111) lattice plane fringes.

is +0.124 V, suggesting that it is more difficult to reduce and requires more extreme conditions.[3,23]

Even though great progress has been made on the size control of Ge NCs, control of crystallinity is not as well-developed because of the strong covalent nature of the Ge−Ge bond. The crystallite size calculated from X-ray diffraction (XRD) is commonly reported to be significantly smaller than the particle size measured from transmission electron microscopy (TEM) images.[21,24−29] This observation may be attributed to an amorphous or reconstructed Ge surface giving rise to a larger particle size in TEM as well as the polycrystalline nature of the NCs. Ge NCs with high crystallinity should be well-capped with surface ligands providing less defects at the surface, and enhancing carrier mobility and photoluminescence and may be further beneficial to the application of various electronics.

Herein, a two-step microwave-assisted solution synthesis route is designed and processed. Pristine Ge NCs with different sizes were synthesized from GeI_4 and investigated with temperature, reaction duration, and concentration. As-synthesized Ge NCs are characterized by powder XRD, TEM, high-angle annular dark-field scanning transmission electron microscopy (HAADF-STEM), and selected area electron diffraction (SAED). NMR spectroscopy, high-resolution mass spectrometry (HRMS), and gas chromatography (GC) were applied to analyze and understand the liquid and gas phases of the reaction. This work demonstrates a new route synthesizing single-crystalline Ge NCs with enhanced quality, which could be further developed for applications. The studies on this two-step reaction provide insight to improve the nanocrystal synthesis not only for Ge but also for other covalently bonded semiconductors or metals.

2. RESULTS AND DISCUSSION

2.1. Synthesis and Characterization

In this work, we designed a two-step microwave-assisted colloidal reaction to prepare highly crystallized Ge NCs by the reaction of OAm with GeI_4. In brief, in a typical synthesis of Ge NCs, a stock solution of GeI_4 in OAm was heated with a CEM microwave reactor under Ar(g) at 250 °C for 40 min. A power of 150 W was applied to provide a moderate ramping rate. A pressure of 40 psi was detected in the microwave tube indicating the formation of gases during the synthesis process. We noticed the pressure produced is correlated with the process of this step. A light-yellow solution obtained after the first step indicated the possible formation of a Ge(II) species. We did not observe a significant Tyndall effect in the resulting solution nor any observable nucleation of Ge particles under TEM.

The head gas from the initial yellow solution was removed and replaced with Ar(g), and then, the vessel was heated again by microwave to 260 °C and held for various lengths of time.

https://doi.org/10.1021/acsmaterialsau.1c00072
ACS Mater. Au 2022, 2, 330−342

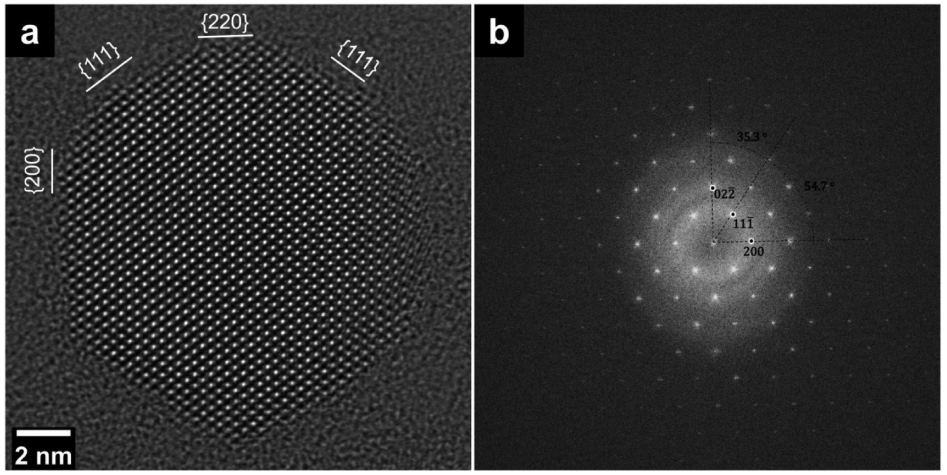

Figure 2. (a) Atomic resolution of one as-synthesized Ge NC via the two-step method from GeI_4. The image shows high crystallinity and the single-crystal nature of the NC. Facets of the NC are labeled. (b) Corresponding Fourier transform of the image (a).

After cooling to room temperature, a brown-colored solution indicated the successful formation of Ge NCs. The product was isolated by the widely used solvent/nonsolvent method as described in the Experimental Methods. The precipitated product was dispersed in toluene for further characterization.

Reactions were stopped at 5, 15, and 30 min at 260 °C in the second step to determine the growth process. Brown-colored products were obtained in all reactions. Representative dark-field STEM (DF-STEM) images of different reaction times are shown in Figure 1a−c. The particle size becomes larger, and the size distribution range becomes smaller with a longer reaction time in the second step. At the early stage (5 min reaction), both small (∼6 nm) and large (∼18 nm) particles were observed, which indicates quick nucleation and growth. The uniformity and size of particles increased as the reaction proceeds, while the small particles (<10 nm) disappeared. This indicates an Ostwald ripening process where the large particles grow at the cost of the small ones. No small particles were observed after 30 min, indicating the nucleation process was terminated at a certain point during the reaction. Over 200 Ge NCs were selected randomly to calculate the size distribution histograms of these three different stages of reaction as shown in the Supporting Information (SI), Figure S1. After 30 min of reaction, the average particle size is 18.9 ± 1.84 nm, with less than 10% dispersity. The as-synthesized NCs show explicit particle edges in the DF-STEM image. The quality of these images is significantly improved compared with our previously published work where NCs are obtained by reducing GeI_2 in OAm.[24,25,30] Particles prepared with GeI_2 in OAm showed vague edges around the particles in the HAADF-STEM images, which were attributed to the amorphous layer on the surface of the NCs.[24,25,30] Similar results are also reported in several other studies on solution-synthesized Ge NCs, demonstrating the difficulties of making Ge NCs with high crystallinity.[3,31] The corresponding selected area electron diffraction (SAED) pattern (inset of Figure 1c) matches the expected pattern for the crystalline diamond cubic structure of Ge. The high intensity of the SAED rings further verifies the high crystallinity of the NCs. High-resolution transmission electron microscopy (HRTEM) (Figure 1d) shows clear lattice fringes on several NCs without any interfaces, indicating the single-crystal nature, and the *d*-spacing was calculated to be 0.335 nm, which is consistent with the lattice spacing of the diamond cubic Ge (111) phase. An atomic-resolution TEM image with edge identification (Figure 2a) of one Ge NC demonstrates the high crystallinity and single-crystal nature. A corresponding FFT image is shown in Figure 2b. Other high-resolution TEM images are provided in the SI (Figure S2). Most of the as-synthesized Ge NCs are single-crystal with some NCs showing lattice interfaces indicating a possible twin defect in the NC (SI, Figure S2g−i).

The PXRD pattern (Figure 3) shows a pure phase of cubic diamond-structured Ge NCs. Diffraction peaks at 27.3, 45.4,

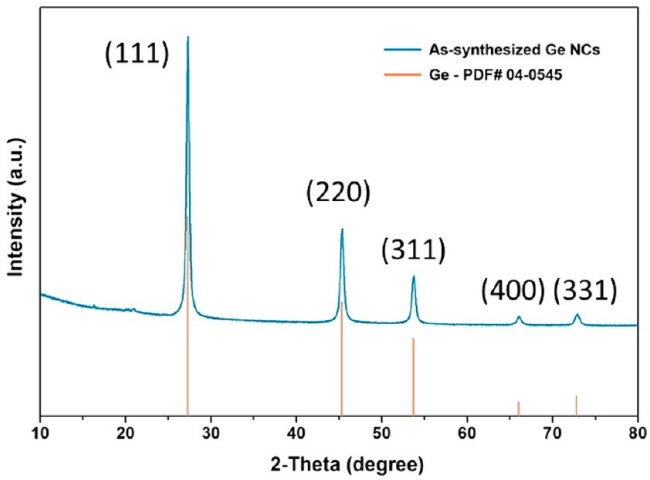

Figure 3. PXRD pattern of the Ge NCs synthesized at 260 °C for 30 min compared to the reference pattern (PDF #04-0545) showing the (111), (220), (311), (400), and (331) reflections of cubic Ge.

53.8, 66.1, and 72.9° two-theta correspond to the (111), (220), (311), (400), and (331) lattice planes, respectively. The sharp peaks and high signal-to-noise ratio indicate the high crystallinity of the as-synthesized Ge NCs. The crystallite size was calculated by the Scherrer equation for the peak broadening of the (220) peak instead of (111) to eliminate errors from peak asymmetry and background removal.[22,31] A crystallite size of 16.5 nm obtained by the Scherrer equation is very similar to the particle size calculated by TEM. As the Scherrer equation tends to underestimate the particle size

https://doi.org/10.1021/acsmaterialsau.1c00072
ACS Mater. Au 2022, 2, 330−342

when prominent size dispersions exist, the similar particle sizes calculated by two different methods indicate the high crystallinity and monodispersity of the Ge NCs prepared by this method.[31,32]

To compare with the two-step reactions, a one-step reaction of the same amount of GeI_4 stock solution was carried out by microwave heating at 250 °C. After 1 h holding at the set temperature, a dark-brown- to black-colored product was obtained. This reaction shows that GeI_4 can be reduced by OAm without the assistance of any other reducing agents. The dark color indicates a large particle size of the Ge NCs. The same isolation process as described above was followed. Rather than well-dispersed NCs, the TEM images of the product (SI, Figure S3a) show agglomerates of around 100 nm in diameter. The as-synthesized sample is unable to form a stable colloidal solution, which is attributed to the poor ligand capping and thereby formation of agglomerates. The agglomerates are formed with many small crystalline nanoparticles as shown in SI, Figure S3b. This suggests a fast nucleation process as well as poor ligand capping. While the reaction happens in a short period with continuous heating, the small Ge NCs formed at the early stage aggregate together directly rather than continuing to grow into larger NCs. Similar results were reported in other work involving GeI_4.[3,22] The advantage of the two-step reaction is that it prevents the uncontrolled aggregation and provides a homogeneous Ge NCs colloid.

To investigate the relationship between concentration and particle growth, various concentrated stock solutions (17.5, 35, and 70 mM) were prepared as described in the Experimental Section. The same reaction process was carried out on these different concentrated stock solutions. The reactions were all held at the set temperature for 30 min for the second step. We noticed that with higher concentration, it took a shorter time to reach the set temperature in both steps. The relation of time required to reach the set temperature versus the solution concentration of both the first and second steps is plotted in Figure 4a. Heating profiles of these reactions are plotted in Figure 4b. It has been shown that the nonpolar OAm is a poor microwave absorber.[21,22] The heating rate of the solution relies on the type and concentration of precursors and the volume of solution. GeI_4 has been observed to be a better microwave absorber than GeI_2 due to the formation of ionic and possibly polar species.[21] In this work, the same volume of OAm solvent is used in all parallel reactions, and GeI_4 serves as the single Ge source. Thus, the heating rate is controlled by precursor concentrations.

We noticed that to obtain a yellow solution after the first step, a much longer holding time is required for stock solutions with lower concentration, which is consistent with the ramping profile shown in Figure 4b. A standard (35 mM) stock solution turned yellowish after 40 min of reaction, while a double-concentrated solution (70 mM) became darker yellow after only 20 min. For comparison, a half-concentrated solution (17.5 mM) could only achieve a pale-yellow color even after 80 min of reaction, which might be due to an insufficient microwave energy absorber in the solution. Those different colors were shown in the SI, Figure S4. A freshly prepared Ge stock solution and pure OAm were also provided as a reference. All the three yellow solutions after the first step were transferred into the glovebox, and 2 mL of each was reloaded into a new microwave tube with a rubber cap and PTFE liner and transferred out from the glovebox for the next reaction step.

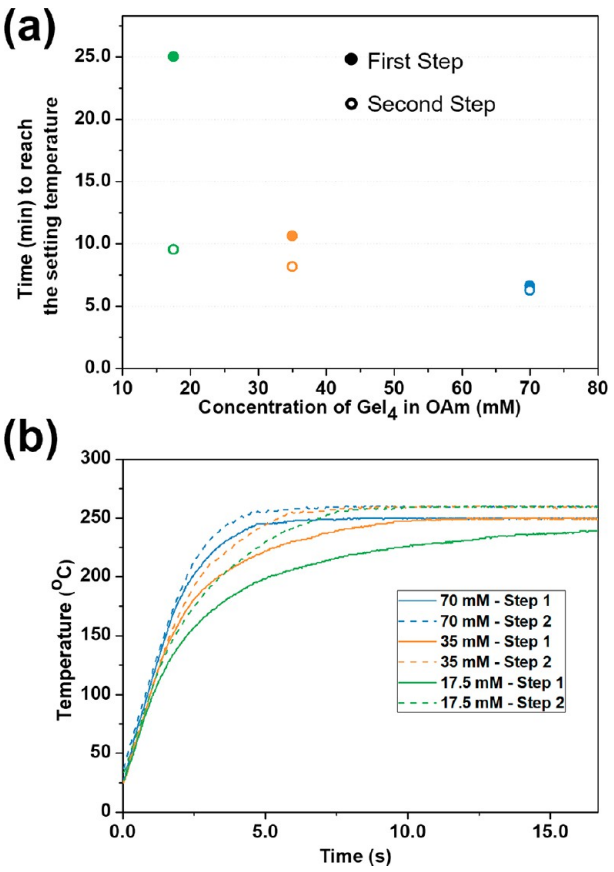

Figure 4. (a) Time required to reach 250 °C for the first step and 260 °C for the second step versus different concentrations of GeI_4 OAm solution. (b) Temperature profiles for microwave heating of reactions with different concentrations of GeI_4.

The three microwave tubes were heated and held at 260 °C for 30 min sequentially in the microwave reactor, and products were isolated from all three different concentrations. Figure 5 displays the HADDF-STEM images of Ge NCs synthesized with different GeI_4 concentration stock solutions after the second step. Statistic histograms are reported in the SI, Figure S5. Half-concentrated stock solution (17.5 mM) gave an NC average size of 11.9 ± 1.89 nm, much smaller than that of standard concentrated (35 mM) solution (18.9 ± 1.84 nm). This suggests that the less concentrated solution contains less molecular precursors, which reduces the growth rate and in turn limits the particle size. With the same reaction time of the second step, the particle size distribution range of the sample prepared from the half-concentrated solution is wider than that from the standard concentration solution. This observation on the sample prepared from the half-concentrated solution indicates that the growth process is slow and not finished after 30 min due to the low concentration of the Ge precursors. We extended the reaction time to 45 min for the second step of the half-concentrated sample. The NCs size increased to 14.5 nm, and the size dispersity also improved to a narrower range indicating an Ostwald ripening process in this step. The HADDF-STEM image and corresponding histogram are shown in the SI, Figure S6. Interestingly, the particles from the double-concentrated (70 mM) solution were aggregated together (Figure 5c) and show a similar structure and morphology to that of the particles synthesized by a one-step reaction (SI, Figure S3a). High-concentration stock solution

https://doi.org/10.1021/acsmaterialsau.1c00072
ACS Mater. Au 2022, 2, 330−342

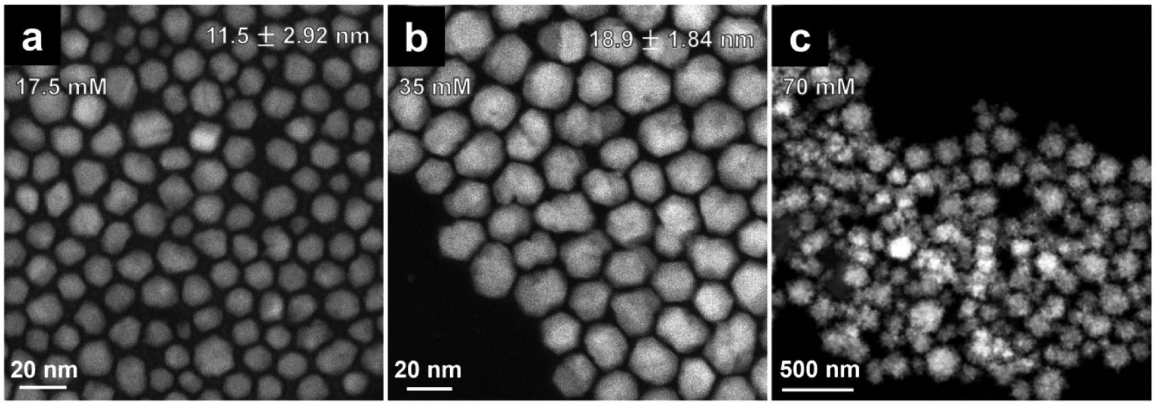

Figure 5. HADDF-STEM images of Ge NCs synthesized with different GeI_4 concentration stock solutions after the second step at 260 °C for 30 min. Stock solutions with GeI_4 concentrations of (a) 17.5 mM, (b) 35 mM, and (c) 70 mM.

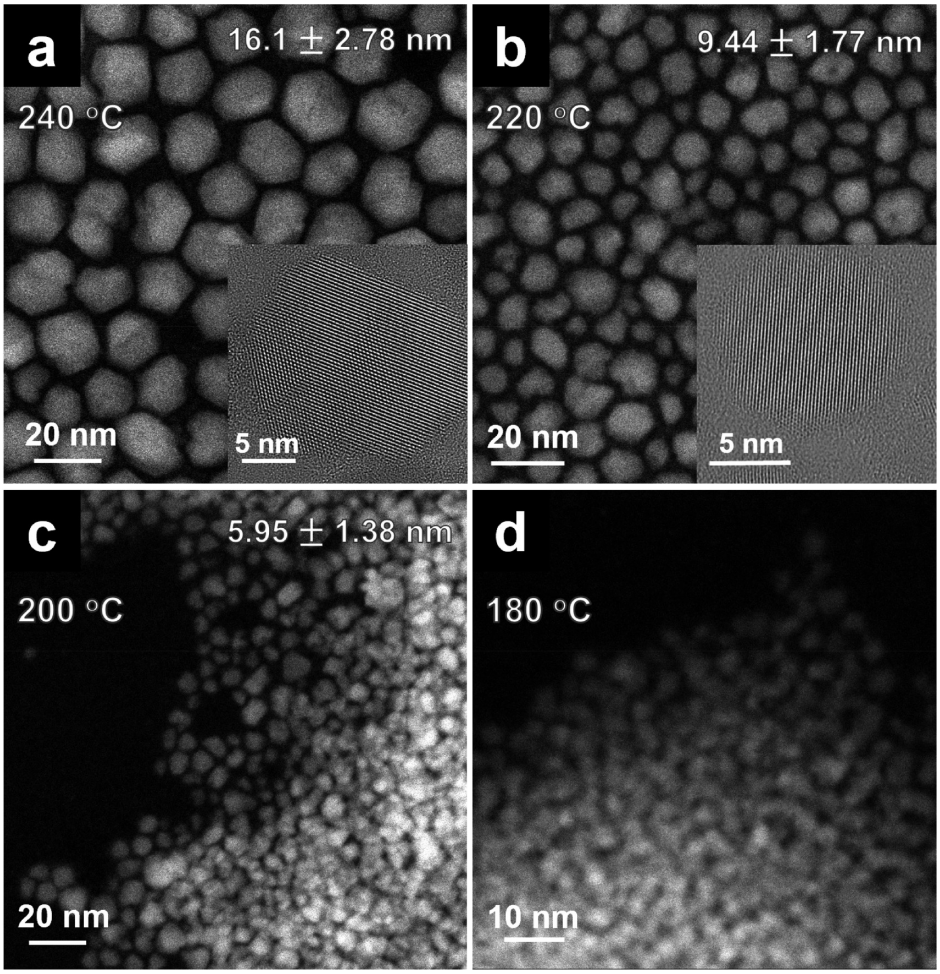

Figure 6. DF-STEM images of Ge NCs synthesized at different reaction temperatures of the second step: (a) 240 °C, (b) 220 °C, (c) 200 °C, and (d) 180 °C.

kinetically improved the reaction rate. However, the particles are formed with poor lattice alignment and ligand capping due to the fast nucleation and growth rate. The small particles aggregated to make large agglomerates with sizes over hundreds of nanometers.

Reactions with different times and concentrations were explored and discussed above. Increasing the reaction time for a solution with a suitable concentration moderated the growth and ripening of the Ge NCs. Another factor that may affect the growth of the nanoparticles is the temperature. Here, different reaction temperatures for the second step were investigated to further understand the nucleation and growth processes. Besides 260 °C, reactions were also carried out at 240, 220, 200, 180, and 160 °C for the second step. To provide enough reaction time for particle ripening at lower temperatures, samples were all held 45 min at these temperatures. Brown-colored products were all successfully obtained, indicating the nucleation and growth could happen at temperatures as low as

https://doi.org/10.1021/acsmaterialsau.1c00072
ACS Mater. Au 2022, 2, 330−342

160 °C. However, the yield of Ge NCs after 45 min at 160 °C is very low. A low-temperature synthesis of Ge NCs was also recently reported for the thermolysis of a bis(amidinato)-germylene(II) complex and suggests that these species might be present in the reaction mixture after the initial heat treatment.[33] To the best of our knowledge, this is the first example of high-quality colloidal Ge NCs being prepared at a temperature lower than 200 °C in organic solvent media without any additional reducing agents and suggests further research to determine whether small Ge-contained molecular clusters may be participating in this reaction as is noted for other semiconductor nanoparticle growth, such as the case of InP.[34]

Figure 6 displays Ge NCs synthesized at different temperatures with the corresponding size histograms shown in SI, Figure S7. As expected, the particle size decreased with a lower heating temperature. When the temperature is lower than 220 °C, aggregation occurs as shown in Figure 6c,d, which is attributed to the poor surface capping of OAm. The role of OAm as a capping ligand on the surface of Ge has been previously studied by NMR.[35] This study showed that OAm on the surface of Ge can be transformed from an L-type amine ligand to a much stronger X-type ligand of oleylamide, the fraction of which increased with increasing temperatures.[35] The stronger binding X-type of ligands result in more stable capped NCs and colloidal suspensions. The particle boundaries became indistinct with low temperatures indicating that either insufficient heating produced an amorphous Ge surface or possibly that the dative bonding of the L-type ligand allows for surface reconstruction by reaction with oxygen/water and thereby amorphization. The NCs synthesized at 240 and 220 °C show high crystallinity and a single-crystal nature as shown in the inset images of Figure 6a,b. With a different reaction temperature for the second step, we can tune and control the size of the synthesized particles.

2.2. Photothermal Deflection Spectroscopy (PDS) and Photocurrent Measurements

Photothermal deflection spectroscopy (PDS) is used as a sensitive measurement of band-to-band absorbance. In brief, the thin film is placed securely in a quartz cuvette filled with Fluorinert FC-72 (3M).[24,36] The sample's surface is then aligned with the probing beam of a 2 mW He−Ne laser. Normal to the surface, the sample is pumped by monochromatic light modulated at 5 Hz. This modulation allows the sample's optically excited charge carriers to nonradiatively relax and release heat. This heat is absorbed by the Fluorinert, which is known for having an index of refraction that is sensitive to temperature. Therefore, the heat released by increased absorbance leads to the probing beam's path through the cuvette deviating further from a straight line, and this deviation is measured by a position-sensitive light detector. This allows for an indirect measurement of absorption, without interference from reflected or scattered light.

To investigate how improved crystallinity affects the optoelectronic properties of the Ge NCs, neat thin-films of GeI_2-reduced NCs and GeI_4-reduced NCs were prepared for PDS, as shown in Figure 7. The GeI_2-reduced NCs with an average size of 9.76 ± 1.98 nm were synthesized following published work and described in detail in the Experimental Section.[21,24] The GeI_4-reduced NCs were synthesized via the two-step reaction reported in this work. Two samples of GeI_4-reduced NCs were measured to be 10.2 ± 2.21 and 18.1 ± 1.78 nm, respectively. The HADDF-STEM images of Ge NCs measured with PDS are shown in Figure 8. Corresponding XRD patterns of these three samples are presented in the SI, Figure S8, and the crystal sizes were calculated with the Scherrer equation. While the 10 nm Ge NCs from GeI_2 and GeI_4 had a similar particle size, the broader peaks in the XRD pattern of GeI_2-reduced NC sample indicate a smaller overall crystal size. This could be attributed to a higher degree of the amorphization of the Ge NCs surface of GeI_2-reduced sample.

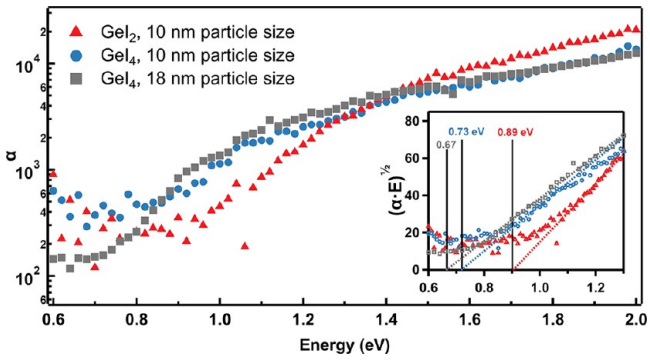

Figure 7. PDS measurements of 10 nm GeI_2-reduced, 10 nm GeI_4-reduced, and 18 nm GeI_4-reduced Ge NCs. Inset is the Tauc plot with the estimation of indirect bandgaps of these three Ge NC samples.

Bandgap estimates were made through linear fits of a Tauc plot by $(\alpha \cdot E)^{1/2}$ for indirect semiconductors. The x-intercept of the linear fit of the midgap region provides an estimate of the bandgap energy. Fits to Tauc plots indicate the energetic bandgap to be 0.89 ± 0.05 eV for GeI_2 NCs and 0.73 ± 0.03 eV for GeI_4 NCs with similar particle sizes around 10 nm (Figure 7, inset). The simulated bandgap of Ge NCs from GeI_2 matches well with the reported data of Ge NCs with similar sizes.[22,24] While the particle sizes in each sample were similar, the GeI_2-reduced NCs have a smaller crystalline core, which is attributed to the lesser crystallinity and amorphous layer on the surface, decreasing the effective confined space an electron experiences and thus increasing the bandgap in the material. The more bulk-like bandgap of the GeI_4-reduced NCs indicates that the quantum confinement effects associated with NCs is strongly dependent on the crystallite size, as measured by XRD, rather than the particle size measured in TEM. Tauc fits to the larger 18 nm GeI_4-reduced NC samples show a more bulk-like bandgap of 0.67 ± 0.02 eV. The increased accuracy for our larger-sized samples is likely due to the narrower size distribution, as described above. Ruddy et al. showed similar bandgap trends with increasing particle size, though direct comparisons are difficult, as they did not estimate the size of their crystalline core.[3]

The Urbach energy of a sample is a measure of disorder and may be due to surface states, structural disorder, or doping. Additional disorder in NC and quantum dot systems is consequent from the increased surface area and size dispersion. For reference, crystalline silicon has been measured to have $E_{Urbach} < 20$ meV, amorphous silicon has $E_{Urbach} \approx 45$ meV, and CdSe QDs have an E_{Urbach} of up to 200 meV.[37,38] This disorder results in energy states available below the band edge, represented by an exponentially decreasing absorption coefficient $\alpha \approx \alpha_0 \exp(E/E_{Urbach})$ below the bandgap edge. As shown in SI, Figure S9, Urbach energies for the similarly sized GeI_2-reduced and GeI_4-reduced Ge NCs were both 145 ± 5 meV, while the 18 nm GeI_4 sample has a smaller Urbach

https://doi.org/10.1021/acsmaterialsau.1c00072
ACS Mater. Au 2022, 2, 330−342

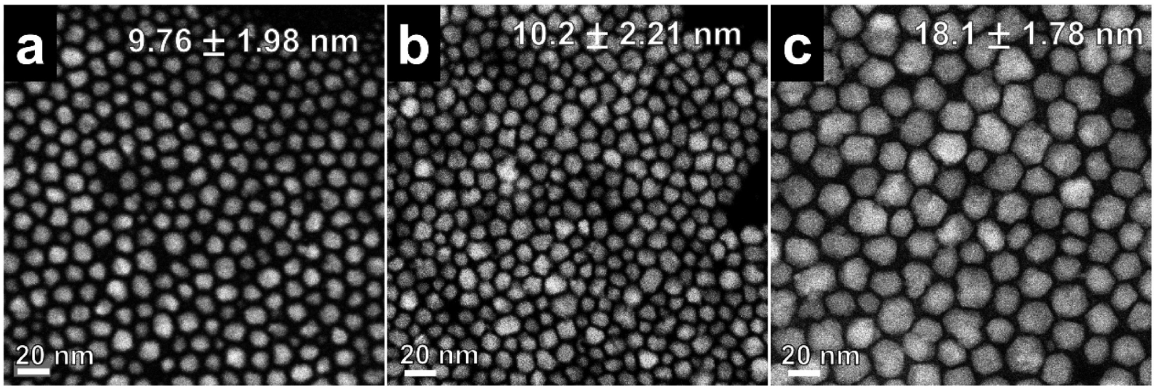

Figure 8. HADDF-STEM images of (a) 10 nm GeI_2-reduced Ge NCs from a modified one-step reaction and (b) 10 nm GeI_4-reduced and (c) 18 nm GeI_4-reduced Ge NCs synthesized by the two-step reaction reported in this work.

energy of 95 ± 5 meV. This indicates that disorder might correlate with the fraction of surface states associated with decreased particle size or perhaps the increased molar ratio of ligands to germanium, rather than the crystallinity of the individual nanocrystal.

To investigate our synthesis method's impact on conductivity, we fabricated heterojunction thin-film optoelectronic devices, using Ge NCs that were made from either GeI_2 or GeI_4 solutions as the active layer. To control for interparticle spacing, both NC samples were prepared to have an average particle size of about 10 nm. All devices used a compact blocking TiO_2 layer (c-TiO_2), followed by a mesoporous TiO_2 layer (m-TiO_2) that aids in electron extraction. NC solutions were spin-coated atop these layers, with Ag capping the devices (Figure 9, inset). Figure 9 shows average photocurrents for a

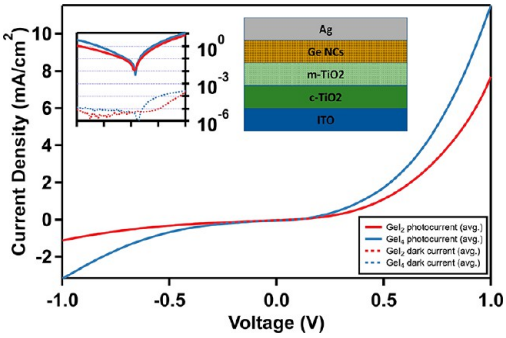

Figure 9. Average photocurrents for a set of devices prepared from GeI_2-reduced and GeI_4-reduced Ge NCs with similar average sizes. The inset displays the semilog plots of both photocurrent and dark currents. And a scheme image of the as-fabricated device is presented as the right inset.

set of GeI_2 and GeI_4 devices, with the inset displaying semilog plots of both photocurrent and dark currents. The actual photocurrents plots are shown in SI, Figure S10. A comparison of the average photocurrents extracted from our devices suggests increased performance in conductivity. It has been shown in perovskite heterojunction planar devices that increased crystallinity of the active layer leads to increases in photocurrent.[39] Similarly, the improved crystallinity in the GeI_4-reduced Ge NC samples likely leads to a reduction in trap states and an overall improvement in charge extraction. Photocurrents showed a five-decade change in magnitude in comparison to dark currents, a favorable characteristic for photodetectors.

2.3. Mechanistic Investigation of the Two-Step Reaction

OAm is a widely employed capping ligand that prevents aggregation, coalescence, and termination of particle growth.[3,21,22,35,40] As mentioned previously, Smock et al. systematically studied the surface of solution-synthesized Ge NCs by NMR and concluded that the strongly bound native ligands are X-type Ge−NHR covalent bonds whose fraction increased with higher reaction temperature.[35] When it comes to redox mechanisms involving OAm, different viable pathways have been proposed.[3,41−44] It has been reported that when OAm is the only reducing agent in the reaction, the lone pair of electrons in the amine group is necessary for the reduction process[45] and the carbon double bond in OAm is not playing a significant role in the reactions.[46] In some syntheses of metal nanoparticles involving OAm and metal oxide precursor, a catalytic hydrodenitrogenation reaction occurs and results in a cleavage of C−N bond of the amine.[44] Amino radicals formed at a relatively high temperature could transform to imine or nitrile through deprotonation reaction.[41] Tabatabaei et al. proposed a different pathway for the reducing process to form Ge NCs by OAm with the formation of hydrogen gas. Supported with FT-IR and NMR, there was no evidence for the existence of imine nor nitrile groups to serve as capping ligands on the surface of Ge NCs.[22]

Ruddy et al. reduced mixed valence Ge precursors, GeI_2 and GeI_4, to synthesize Ge NCs with the assistance of a reducing agent, BuLi.[3] It was proposed Ge(IV) could also be reduced to Ge^0 at a relatively high temperature (>250 °C).[3] In this work, another pathway is discovered showing that Ge(IV) can be reduced to Ge(II), which is then further reduced to Ge^0. We investigated possible mechanisms behind the reactions of germanium precursors with OAm employing MS, GC, and NMR.

High-resolution mass spectrometry (HRMS) in the SI, Figure S11, shows OAm, the GeI_4 stock solution and the GeI_2 stock solution as well as these solutions after the first microwave heating, the GeI_4 stock solution after the second heating, along with an OAm + I_2 solution after heating. Table 1 summarized the major HRMS peaks and possible species. The OAm solution shows a typical mass spectrum with the main peak at 268.30 m/z. The GeI_4 stock solution shows the OAm peak and two new peaks: an exact mass of 663.5 amu, which could be assigned to an ammonium−iodide complex

https://doi.org/10.1021/acsmaterialsau.1c00072
ACS Mater. Au 2022, 2, 330−342

Table 1. High-Resolution Mass Spectrometry Peaks and Possible Species[a]

m/z; z = 1	empirical formula	formula change from parent	possible species
268.2998	$C_{18}H_{38}N$	OAm	R′−CH_2−NH_2
516.5506	$C_{36}H_{70}N$	2*OAM − NH_3 − 2*H	R′−CH=N−CH_2−R′
518.5617	$C_{36}H_{72}N$	2*OAM − NH_3	R′−CH_2−NH−CH_2−R′
663.5053	$C_{36}H_{78}N_2I$	2*OAM + I + 2*H	$((RNH_3)_2I)^+$

[a]Here, R′ is $CH_3(CH_2)_7CH{=}CH(CH_2)_7^-$.

$((RNH_3)_2I)^+$, and 516.55 amu, which could be assigned to an imine group R′−CH=N−CH_2−R′. Here, R′ is $CH_3(CH_2)_7CH{=}CH(CH_2)_7^-$ as the same carbon chain in OAm without the NH_2CH_2− group. These two peaks are also seen in a GeI_2 stock solution at room temperature in SI, Figure S11c. It is unexpected that an imine formed at room temperature in the GeI_4 stock solution. The possibility should be considered that the imine could be produced in the MS via an intense gas phase process.[47] However, after the first heating of the GeI_4 stock solution, a peak with 518.56 m/z arises, indicating the presence of the product of the dimerization of OAm, $((CH_3(CH_2)_7CH{=}CH(CH_2)_7CH_2)_2NH)$. During the heating reaction, ammonia gas is produced, identified by GC; see below. The peak intensity of the 518.56 m/z increased dramatically after the second heating process (SI, Figure S11e) demonstrating a higher degree of dimerization. The same MS peak (518.56 m/z) was reported for a GeI_2 microwave reaction.[22] The MS signal provides evidence that the Ge(IV)/I^- ions might play an important role in the formation of an imine group at room temperature, and the I^- ion triggers the dimerization reaction of amines.

Gas chromatography (GC) was also used to qualitatively determine the gases produced during both steps of the reaction by injecting the gas taken from the headspace of the sealed microwave tubes. In both steps, H_2 and NH_3 gas were detected, confirmed by the pure gas injection as a comparison (SI, Figure S12). The formation of NH_3 is consistent with the MS data of the formation of the OAm dimer. The pathway of the production of H_2 gas during the reaction is still unsolved. One possible hypothesis is that H_2 is released from the deprotonation reaction of OAm induced by I^-.[22] Another possible pathway is that the amine could undergo a nucleophilic substitution reaction with protonated amine (ammonium), followed with a dehydrogenation reaction.[47] Both NH_3 and H_2 gases were produced in this process.

The function of H_2 gas in the reaction was investigated by running a reaction with conventional heating. The yellow solution obtained after the first-step microwave heating was transferred into a flask. The flask was heated by a heating mantle and assembled with argon gas flow to remove the

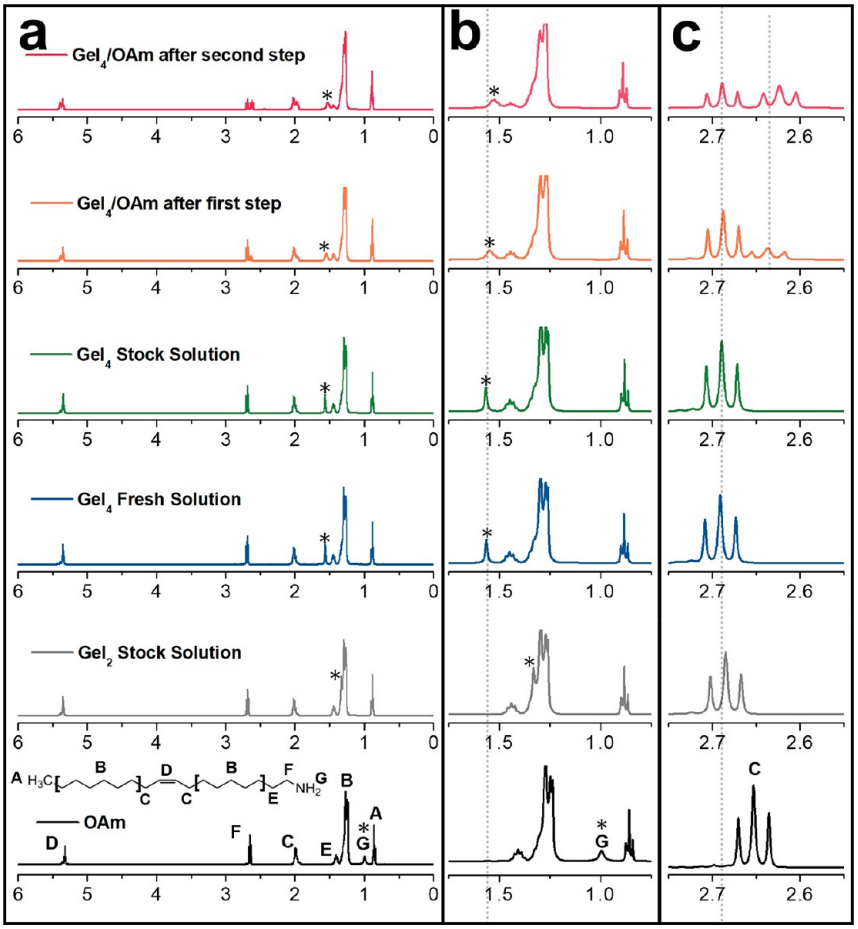

Figure 10. (a) Overall NMR spectra of degassed OAm, GeI_2 stock solution, GeI_4 fresh solution and stock solution, and the supernatant of GeI_4/OAm after first and second steps of the reaction. (b) Enlarged spectra with the range of 0.75−1.75 ppm. (c) Enlarged spectra with the range of 2.55−2.75 ppm.

https://doi.org/10.1021/acsmaterialsau.1c00072
ACS Mater. Au 2022, 2, 330−342

produced gases. After 30 min holding at 260 °C, a brown solution was obtained, demonstrating the formation of Ge NCs. As indicated previously, while GC shows the production of H_2(g), it is not the reducing agent for the formation of Ge nanoparticles.[22]

^{1}H NMR spectra (Figure 10a) was obtained from different solutions to study the chemical changes during the reaction. The spectra of the GeI_2 and GeI_4 stock solutions as well as freshly prepared GeI_4 solution and GeI_4 solution after first and second reaction steps are compared with OAm in Figure 10b. In the order of OAm to GeI_2 stock solution to GeI_4 stock solution, the peak corresponding to the amine proton (labeled with *) moves downfield. Shifting of the amine protons with protonation has been previously observed, for example, in a mixture of sulfur and octylamine assigned to the formation of $(RNH_3^+)(RNH{-}S_8^-)$.[48] The amine group of OAm has been reported to serve as an electron donor (L-type) ligand and coordinates with transition metal ions to form a reactive precursor.[49,50] Ge(IV) is a hard Lewis acid according to the hard and soft acid and base (HSAB) theory. Iodide, I^-, compared with an amine group, is soft. Thus, when GeI_4 dissolved in OAm, I^- ligands are partially substituted by OAm, and $[Ge(OAm)_xI_{4-x}]^{x+}$ forms. In the presence of I^-, the amines could undergo a protonation process and form oleylammonium iodide as indicated by the shifting of amine proton peak in the NMR. GeI_2 in OAm undergoes the same process. However, compared with Ge(IV), Ge(II) is comparatively soft due to the larger atomic radius and only possesses two coordinative positions and hence a lower degree of protonation. The peak shift in ^{1}H NMR also correlates with the existence and intensity of the protonated amine peak observed in the MS (SI, Figure S11b). Compared with the OAm reference, the amine proton peak is sharper in precursor stock solutions and attributed to the coordination between Ge(IV) and OAm that reduces the amine−amine interaction. The protonation is a fast process as the amine proton peak of a freshly prepared GeI_4 solution shows the same chemical shift as that of the GeI_4 stock solution.

An extra peak with small upfield shift from the original position of OAm is clearly exhibited in the enlarged range of 2.5−2.8 ppm in the NMR (Figure 10c). The new peak with a upfield shift that is smaller than 0.1 ppm is likely from a derivative product of OAm such as the dioleylamine that is identified by MS. The increasing intensity of this NMR peak correlates with the increasing amount of dioleylamine after the two-step reaction. The proton peaks of the amine broaden and shift slightly upfield after the two-step heating. The broadening is caused by multiple environments of amine. The shifting is attributed to the formation of dioleylamine, which has a more shielded amine group. Detected and presumed species are summarized in Table 2 according to MS, GC, and NMR.

Table 2. Summary of Detected and Presumed Complexes and Species from NMR, MS, and GC

	NMR	MS	GC
GeI_4 stock solution	$[Ge(OAm)_xI_{4-x}]^{x+}$; RNH_3^+	R′−CH═N−CH_2−R′; $((RNH_3)_2I)^+$	-
GeI_4/OAm after first step	dioleylamine	dioleylamine	NH_3; H_2
GeI_4/OAm after second step	dioleylamine	dioleylamine	NH_3; H_2

Based on the summarized species, we propose a possible mechanism for the reduction of Ge(IV) to Ge(II) in OAm. It was reported decades ago that Ge(IV) can be easily reduced by different amines such as ethylamine and aniline.[51−53] The reaction pathways are listed below in eqs 1 and 2. Followed by the disproportion reaction (eq 3), Ge undergoes nucleation and growth under the control of the concentration of Ge(IV).

$$[Ge(NH_2CH_2R')_4]^{4+} + 4NH_2CH_2R' \rightarrow Ge(NHCH_2R')_4 + 4(NH_3CH_2R')^+ \quad (1)$$

$$Ge(NHCH_2R')_3 \rightarrow Ge(N{=}CHR)_2 + 2NH_2CH_2R' \quad (2)$$

$$Ge(II) \leftrightharpoons Ge^0 + Ge(IV) \quad (3)$$

The proposed reduction mechanism is similar to that reported in Nam's work on the synthesis of cobalt nanoparticles.[44] The possible reaction pathways are shown in Scheme 1. The OAm deprotonates to form a stronger coordinating ligand, oleylamide. The α-carbon atom of the coordinated oleylamide ligand on Ge(IV) interacts with the relatively electronegative nitrogen atom in another oleylamide ligand binding on the same center Ge atom. This results in the cleavage of the N−C bond, also known as the denitrogenation reaction. The subsequent reaction undergoes a β-hydride elimination, which forms an imine and Ge hydride bond. The Ge(IV)−amine−hydride complex will be quickly reduced to Ge(II) with the formation of NH_3 gas, which is observed in GC. While the imine could react with the observed H_2 gas and form the dioleylamine (R−NH−R) observed in the MS, the Ge(II) species undergoes a disproportion reaction and gives Ge^0 and Ge(IV) as shown in eq 3. In this proposed mechanism, the surface ligand change from OAm to oleylamide is necessary, which reduces the overall reaction rate and prevents aggregation of small Ge nucleus. The NH_3 gas is formed from the fast reductive elimination reaction. Several germanium−amine−hydride complexes have been successfully prepared and stabilized by bulky coordinates.[54] These Ge−amine−hydride complexes are confirmed by single-crystal X-ray diffraction, and further efforts on short chain amines might provide further insight.[54]

In this work, a two-step reaction was carried out to synthesize Ge NCs from GeI_4. In the Synthesis and Characterization section, different reactions demonstrate that the reaction rate is responsible for the nucleation, growth, and dispersion of the as-synthesized Ge NCs. In a prepared GeI_4/OAm solution, the ligands exchange and form $[Ge(OAm)_xI_{4-x}]^{x+}$. When the solution is heated, binding ligands change from L-type oleylamine to stronger X-type oleylamide (Ge−NHR). Oleylamide is a long chain bulky ligand with strong binding affinity.[35] These two factors decelerate the reaction rate of the center atom, Ge(IV) and control the nucleation and growth of Ge NCs.[43,55,56]

Mixed-valent Ge precursors have been employed to control the size and improve the crystallinity of Ge NCs. It was believed that Ge^0 nucleated from Ge(II) reduction and grew from Ge(IV) reduction at a high temperature.[3] However, in our work, we confirmed that Ge(IV) can be reduced to Ge(II) and then undergo the well-documented disproportion reaction at microwave temperatures of 260 °C and lower, providing Ge^0 and presumably Ge(IV) as shown in eq 3. A high concentration of Ge(IV) in the solution further slows down

https://doi.org/10.1021/acsmaterialsau.1c00072
ACS Mater. Au 2022, 2, 330−342

Scheme 1. Proposed Reaction Pathways for the Reduction of Ge(IV) to Ge(II) by OAm[a]

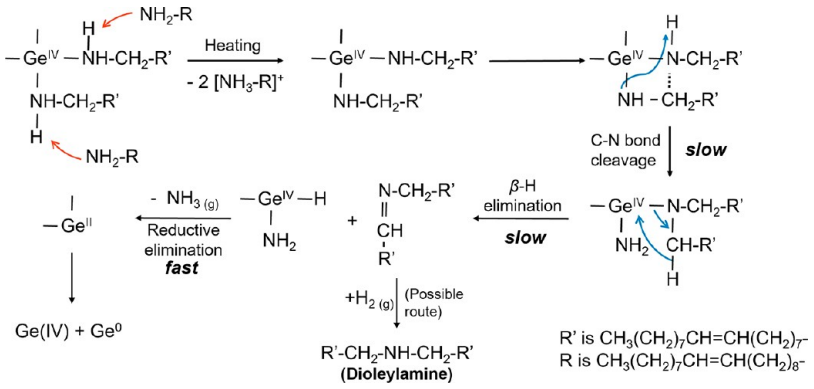

[a]Ge(IV) is reduced to Ge(II) by oleylamide from the deprotonation of OAm, with the formation of NH_3 and dioleylamine.

the disproportional reaction and results in the highly crystalline nature of Ge NCs.

3. CONCLUSIONS

A two-step microwave-assisted solution method was designed to synthesize Ge NCs from GeI_4 as the single Ge precursor. The process was investigated with different reaction times, temperatures, and concentrations. Monodispersed Ge NCs with a large average particle size of 18.9 ± 1.84 nm have been successfully produced through this two-step reaction. Both XRD and HRTEM images showed the high crystallinities of the as-synthesized Ge NCs. A high concentration of GeI_4 precursor or a low temperature of reaction results in large aggregations of small Ge nuclei. Urbach energies and optoelectronic properties of 10 nm Ge NCs prepared from GeI_4 by this two-step method were compared with that synthesized from GeI_2 by a reported method and showed higher crystallinities and better electrical conductivity. The reaction process was investigated by NMR, MS, and GC. A possible mechanism was proposed based on the detected species by these characterizations.

Overall, a new synthetic route to Ge NCs was studied and provided improved qualities of as-made Ge NCs. The synthesis could be further modified and applied not only to Ge-based nanostructures but to other metal and semimetal nanocrystals. The investigation of the possible mechanisms involved in this reaction provides new insights on nanoparticle synthesis of covalently bonding semiconductors.

4. EXPERIMENTAL METHODS

4.1. Chemicals

Germanium(IV) and (II) iodides, GeI_4 and GeI_2, were purchased from Prof. Richard Blair's laboratory (University of Central Florida) and confirmed to be phase-pure from powder X-ray diffraction. Oleylamine (OAm, (*Z*)-octadec-9-enylamine, technical grade, >50%, TCI America) was degassed under vacuum for longer than 2 h at 150 °C before use. Methanol, toluene (HPLC grade, Fisher Scientific) were purified using a solvent purification system and stored in a glovebox under argon.

4.2. Two-Step Synthesis of Ge NCs

Microwave heating was applied to all Ge NC reactions by employing a CEM microwave reactor (Discover SP) under dynamic mode. GeI_4 stock solution (35 mM) was prepared by dissolving 1.2 g (2.1 mmol) of GeI_4 in 60 mL of OAm and stirring in an Ar-filled glovebox for a few days. The as-made colorless solution was kept in the glovebox until used in reactions. Different concentration stock solutions were prepared following the same process.

In a typical synthesis of OAm-capped Ge NCs, 6 mL of the prepared GeI_4 stock solution was transferred into a 35 mL borosilicate microwave tube (purchased from CEM Corporation). In the first step of a reaction, the microwave tube with the solution, sealed with a CEM Teflon cap, was removed from the glovebox and heated to 250 °C in the microwave reactor with a maximum heating power of 150 W. After 40 min at 250 °C, the microwave tube was automatically cooled to 60 °C by the reactor, and a clear light-yellow solution was observed. Since the microwave cap is not fully airtight, to avoid any contamination with the air, the tube with the as-made yellow solution was parafilmed and transferred into the glovebox. Parafilm is moisture resistant but gas permeable. Thus, during the vacuum, the gases in the headspace should be removed. The microwave tube cap was removed, and 2 mL of the as-prepared yellow solution was transferred to a clean and dry microwave tube. The 2 mL yellow solution was then transferred out and heated to 260 °C for 30 min also with a maximum power of 150 W to finish the synthesis. A caramel brown-colored solution was obtained. Samples for device fabrication were synthesized slightly differently as described in the following section. To isolate the Ge NCs, the microwave tube containing the final product was transferred to an argon-filled glovebox.

In the glovebox, the brown-colored solution was transferred into a 50 mL centrifuge tube, and 2 mL of anhydrous toluene and 3 mL of anhydrous methanol as an antisolvent were added. For the samples with smaller particle size, a total of 10 mL of anhydrous methanol is required for the isolation. The solution in the centrifuge tube was taken out and centrifuged at 5000 rpm (~3500 rcf) at room temperature for 3 min, and then, the tube was transferred back into the glovebox, and the pale-yellow or pale-brown supernatant was discarded. This wash process was carried out two more times in order to fully remove extra free OAm ligands and other impurities. The final precipitation was well-dispersed in 1 mL of toluene and kept in the glovebox for further characterizations. For some characterization, the supernatant after the second step was acquired. After reacting at 260 °C, the as-prepared brown-colored solution was directly transferred into centrifuge tube in the glovebox and then transferred out and centrifuged at 5000 rpm (~3500 rcf) for 5 min. The Ge NCs could be precipitated, and a pale-yellow solution was obtained for further characterization.

4.3. GeI_2-Reduced Ge NCs (10 nm)

The method is modified from previous works.[22,24] GeI_2 (0.2 mmol) was dissolved in 6 mL of degassed OAm by stirring in the glovebox overnight. A yellow solution was obtained once the GeI_2 fully dissolved. The obtained solution was then microwave heated to 260 °C with 150 W of applied power. After a 60 min reaction, the obtained dark brown-colored solution was isolated by the method described above.

https://doi.org/10.1021/acsmaterialsau.1c00072
ACS Mater. Au 2022, 2, 330−342

4.4. GeI_4-Reduced Ge NCs (10 nm)

A 6 mL aliquot of the as-prepared 35 mM GeI_4/OAm stock solution was transferred into a 35 mL microwave tube. The solution went through a two-step reaction as described above, except a set temperature of 240 °C was applied for the second step. A selective isolation was carried out. In the glovebox, the as-obtained brown solution was transferred to a centrifuge tube without adding any solvents. The centrifuge tube was pumped out and centrifuged at 3000 rpm for 3 min followed with the same isolation as described above.

4.5. GeI_4-Reduced Ge NCs (18 nm)

A 6 mL aliquot of the as-prepared 35 mM GeI_4/OAm stock solution followed the procedure above for the two-step reaction. We kept the volume as 6 mL for the second step at 260 °C for 30 min. The same isolation process was carried out.

4.6. Characterization

Ge NC products were characterized by X-ray diffraction, transmission electron microscopy (TEM), scanning transmission electron microscopy (STEM), selected area electron diffraction (SAED), NMR spectroscopy, and gas chromatography (GC).

4.7. X-ray Diffraction (XRD)

XRD patterns were obtained by drop-casting and drying the toluene dispersion of prepared Ge NCs on a quartz substrate holder. The obtained dark brown thin film was then scanned using a Bruker D8 Advance diffractometer (Cu Kα, 40 kV, 40 mA, λ = 1.5418 Å) with a range of 10−80°.

4.8. Transmission Electron Microscopy (TEM) and Dark-Field Scanning Transmission Electron Microscopy (DF-STEM)

Both TEM and DF-STEM samples were prepared by drop-casting the dilute dispersion of Ge NCs in toluene onto lacey carbon supported by a 400 mesh copper grid (Ted Pella). The grids were dried completely to avoid carbon contamination of the vacuum chamber during electron beam irradiation. TEM/DF-STEM images were acquired using a FEI ThemIS 60−300 STEM/TEM (Thermo Fisher Scientific, US) operated at 300 kV at the National Center for Electron Microscopy within the Molecular Foundry in Lawrence Berkeley National Laboratory. The ThemIS is equipped with image aberration corrector optics and a Ceta2 camera (4k × 4k pixels, and 14-bit dynamic range).

4.9. NMR Spectroscopy

Samples for ^{1}H NMR were prepared by transferring 50 μL of sample solution and mixing with 600 μL of $CDCl_3$ solvent under an inert atmosphere. ^{1}H NMR spectra were obtained at room temperature on a 400 MHz Bruker Advance IIIHD Nanobay Spectrometer. Chemical shifts were referenced to residual undertreated $CHCl_3$ (7.26 ppm).

4.10. Gas Chromatography (GC)

A Varian 3800 GC was used to identify the gases produced during the reaction. The instrument is equipped with a thermal conductivity detector and a Carboxen 1010 PLOT fused silica column (30 m × 0.53 mm) (Supelco) using nitrogen (99.999%, Praxair) as the carrier gas. The microwave tubes were parafilmed. A 2 μL volume of gas was taken and injected into the GC by a borosilicate glass syringe.

4.11. High-Resolution Mass Spectrometry (HRMS)

As-prepared solvents or solutions were analyzed by flow-injection analysis into a Q Exactive HF Orbitrap (Bremen, Germany) operated in the centroid mode. Samples were injected into a mixture of 50% methanol and 0.1% formic acid/H_2O at a flow of 200 μL/min. Source parameters were a 4.5 kV spray voltage, a capillary temperature of 275 °C, and a sheath gas setting of 20. Spectral data were acquired at a resolution setting of 100 000 fwhm with the lock mass feature, which typically results in a mass accuracy <2 ppm.

4.12. Photothermal Deflection Spectroscopy (PDS)

Samples were prepared in a nitrogen glovebox. Thin-film samples were prepared by spin-coating our Ge NC colloidal solution on a glass substrate, at 400−1000 rpm for 60 s. While details of this system are similar to previously reported work,[24,36] what follows is a brief description of this spectroscopy technique. The thin film is placed securely in a quartz cuvette filled with Fluorinert FC-72 (3M). Light from a tungsten halogen arc lamp was used to pump the sample. The light was chopped at 5 Hz and scanned from 2.1 to 0.6 eV, in steps of 0.01 eV, by using a Princeton Instruments Acton monochromator, resulting in a pumping signal with a full-width-half-maximum of 15 nm. Using a beam splitter, this pumping light is partially sent into a reference detector, for signal scaling purposes, and partially made to be incident on the sample, normal to the substrate. A 2 mW He−Ne 633 nm laser (JDSU) was aligned parallel to the surface of the sample and used as a probe beam. As the modulated pump beam excites the sample, heat from nonradiative relaxation causes the probe beam to be deflected. The deflection is registered with a Thorlabs PDP90 position-sensitive detector, whose signal is read by a lock-in amplifier to reduce noise and allow for high-sensitivity absorption measurements. The absorbance is given by the expression: $\alpha = -\frac{1}{d}\ln\left(1 - \frac{V_{sig}}{V_{ref}}C_{norm}\right)$, where α is the absorption coefficient, d is the sample thickness, V_{sig} is the signal amplitude from the PSD, V_{ref} is the signal from the reference detector, and C_{norm} is a normalization constant. Bandgap estimates were made through linear fits on the Tauc plot $(\alpha \cdot E)^{1/n}$ vs E, where E is the photon energy and n is a constant that is 1/2 for direct semiconductors and 2 for indirect semiconductors. The x-intercept of the linear fit of the midgap region provides an estimate of the bandgap energy. Urbach energy, a characterization of the collective disorder in the system, was found by fitting to the relation $\alpha \sim \exp(E/E_{Urbach})$ in the midgap region. In practice, the Urbach energy is obtained through a linear fit of $\ln(\alpha)$ vs E, where the best-fit slope is $1/E_{Urbach}$.

4.13. Device Fabrication

All devices were prepared indium-tin-oxide-patterned glass substrates (Thin Film Devices, inc.). Substrates were cleaned with Alconox detergent and deionized water before being placed in 15 min sonication baths of first acetone and then isopropyl alcohol. The compact blocking-layer TiO_2 layer (Solaronix, Ti-nanoxide BL150/SP) was doctor-bladed onto the ITO. It was then dried on a 115 °C hot plate for 5 min before being sintered in an oven at 500 °C for 30 min. Next, the mesoporous TiO_2 layer (Solaronix, Ti-nanoxide T165/SP) was applied, dried, and sintered in the same manner. Next, the Ge NC solutions were spin-coated atop the TiO_2 layers in a nitrogen-filled glovebox at 400 rpm for 45 s. After being dried on a hot plate at 60−80 C for 5 min, the devices were placed in a thermal evaporation chamber built into the glovebox to avoid oxygen exposure. Approximately 60−80 nm of Ag (Kurt J. Lesker) was patterned on our devices at a rate of 1 Å/s. Current density−voltage measurements were made using a Keithley 2400 source meter. During light measurements, devices were exposed to light from a solar simulator (Oriel) passing through an AM1.5 filter. All device measurements were made in the glovebox.

■ ASSOCIATED CONTENT

Supporting Information

The Supporting Information is available free of charge at https://pubs.acs.org/doi/10.1021/acsmaterialsau.1c00072.

Histograms of size distribution of Ge NCs reported in this work; HRTEM images of Ge NCs by a two-step reaction; TEM and HRTEM of a one-step reaction with GeI_4 and OAm; picture shows the different color of the GeI_4/OAm reaction after the first step; XRD patterns of 10 nm Ge NCs reduced from GeI_2 and GeI_4 and 18 nm Ge NCs reduced from GeI_4; Urbach energy fitting;

https://doi.org/10.1021/acsmaterialsau.1c00072
ACS Mater. Au 2022, 2, 330−342

actual photocurrent plots; HRMS spectra and GC spectra (PDF)

AUTHOR INFORMATION

Corresponding Author

Susan M. Kauzlarich − *Department of Chemistry, University of California, Davis, Davis, California 95616, United States;* orcid.org/0000-0002-3627-237X; Email: smkauzlarich@ucdavis.edu

Authors

Zheng Ju − *Department of Chemistry, University of California, Davis, Davis, California 95616, United States;* orcid.org/0000-0002-5411-6952

Xiao Qi − *Department of Chemistry, University of California, Davis, Davis, California 95616, United States;* orcid.org/0000-0003-4884-6454

Roy Sfadia − *Department of Physics, University of California, Santa Cruz, California 95064, United States*

Minyuan Wang − *Department of Chemistry, University of California, Davis, Davis, California 95616, United States*

Emily Tseng − *Department of Chemistry, University of California, Davis, Davis, California 95616, United States*

Elizabeth C. Panchul − *Department of Physics, University of California, Santa Cruz, California 95064, United States;* Present Address: Department of Chemistry, Humboldt State University, 1 Harpst Street, Arcata, California 95521, United States; orcid.org/0000-0001-7899-0129

Sue A. Carter − *Department of Physics, University of California, Santa Cruz, California 95064, United States;* orcid.org/0000-0002-6233-6250

Complete contact information is available at: https://pubs.acs.org/10.1021/acsmaterialsau.1c00072

Author Contributions

§X.Q. and R.S. contributed equally to this work.

Notes

The authors declare no competing financial interest.

ACKNOWLEDGMENTS

This work was supported by the National Science Foundation CHE-1710110. Electron microscopy work at the Molecular Foundry was supported by the Office of Science, Office of Basic Energy Sciences, of the U.S. Department of Energy under Contract No. DE-AC02-05CH11231. We thank Dr. Karen Bustillo at National Center for Electron Microcopy at Lawrence Berkeley National Laboratory for the help with TEM and STEM measurements. E.C.P. was funded by an NSF REU program (DMR-1950907).

REFERENCES

(1) Pillarisetty, R. Academic and Industry Research Progress in Germanium Nanodevices. *Nature* **2011**, *479*, 324−328.

(2) Muthuswamy, E.; Zhao, J.; Tabatabaei, K.; Amador, M. M.; Holmes, M. A.; Osterloh, F. E.; Kauzlarich, S. M. Thiol-Capped Germanium Nanocrystals: Preparation and Evidence for Quantum Size Effects. *Chem. Mater.* **2014**, *26* (6), 2138−2146.

(3) Ruddy, D. A.; Johnson, J. C.; Smith, E. R.; Neale, N. R. Size and Bandgap Control in the Solution-Phase Synthesis of near-Infrared-Emitting Germanium Nanocrystals. *ACS Nano* **2010**, *4* (12), 7459−7466.

(4) Nozik, A. J. Nanoscience and Nanostructures for Photovoltaics and Solar Fuels. *Nano Lett.* **2010**, *10* (8), 2735−2741.

(5) Vörös, M.; Wippermann, S.; Somogyi, B.; Gali, A.; Rocca, D.; Galli, G.; Zimanyi, G. T. Germanium Nanoparticles with Non-Diamond Core Structures for Solar Energy Conversion. *J. Mater. Chem. A* **2014**, *2* (25), 9820−9827.

(6) Ramasamy, K.; Kotula, P. G.; Fidler, A. F.; Brumbach, M. T.; Pietryga, J. M.; Ivanov, S. A. Sn_xGe_{1-x} Alloy Nanocrystals: A First Step toward Solution-Processed Group IV Photovoltaics. *Chem. Mater.* **2015**, *27* (13), 4640−4649.

(7) Wheeler, L. M.; Nichols, A. W.; Chernomordik, B. D.; Anderson, N. C.; Beard, M. C.; Neale, N. R. All-Inorganic Germanium Nanocrystal Films by Cationic Ligand Exchange. *Nano Lett.* **2016**, *16* (3), 1949−1954.

(8) Chockla, A. M.; Klavetter, K. C.; Mullins, C. B.; Korgel, B. A. Solution-Grown Germanium Nanowire Anodes for Lithium-Ion Batteries. *ACS Appl. Mater. Interfaces* **2012**, *4* (9), 4658−4664.

(9) Yuan, F. W.; Yang, H. J.; Tuan, H. Y. Alkanethiol-Passivated Ge Nanowires as High-Performance Anode Materials for Lithium-Ion Batteries: The Role of Chemical Surface Functionalization. *ACS Nano* **2012**, *6* (11), 9932−9942.

(10) Kamata, Y. High-k/Ge MOSFETs for Future Nanoelectronics. *Materials Today.* **2008**, *11*, 30−38.

(11) Seino, M.; Henderson, E. J.; Puzzo, D. P.; Kadota, N.; Ozin, G. A. Germanium Nanocrystal Doped Inverse Crystalline Silicon Opal. *J. Mater. Chem.* **2011**, *21* (40), 15895−15898.

(12) Vaughn, D. D.; Schaak, R. E. Synthesis, Properties and Applications of Colloidal Germanium and Germanium-Based Nanomaterials. *Chem. Soc. Rev.* **2013**, *42* (7), 2861−2879.

(13) Fan, J.; Chu, P. K. Group IV Nanoparticles: Synthesis, Properties, and Biological Applications. *Small* **2010**, *6* (19), 2080−2098.

(14) Carolan, D. Recent Advances in Germanium Nanocrystals: Synthesis, Optical Properties and Applications. *Prog. Mater. Sci.* **2017**, *90*, 128−158.

(15) Lu, X.; Ziegler, K. J.; Ghezelbash, A.; Johnston, K. P.; Korgel, B. A. Synthesis of Germanium Nanocrystals in High Temperature Supercritical Fluid Solvents. *Nano Lett.* **2004**, *4* (5), 969−974.

(16) Tabatabaei, K.; Lu, H.; Nolan, B. M.; Cen, X.; McCold, C. E.; Zhang, X.; Brutchey, R. L.; Van Benthem, K.; Hihath, J.; Kauzlarich, S. M. Bismuth Doping of Germanium Nanocrystals through Colloidal Chemistry. *Chem. Mater.* **2017**, *29* (17), 7353−7363.

(17) McVey, B. F. P.; Prabakar, S.; Gooding, J. J.; Tilley, R. D. Solution Synthesis, Surface Passivation, Optical Properties, Biomedical Applications, and Cytotoxicity of Silicon and Germanium Nanocrystals. *ChemPlusChem.* **2017**, *82* (1), 60−73.

(18) Chou, N. H.; Oyler, K. D.; Motl, N. E.; Schaak, R. E. Colloidal Synthesis of Germanium Nanocrystals Using Room-Temperature Benchtop Chemistry. *Chem. Mater.* **2009**, *21* (18), 4105−4107.

(19) Jeon, Y.; Lee, G. H.; Park, J.; Kim, B.; Chang, Y. Magnetic Properties of Monodisperse NiH_x Nanoparticles and Comparison to Those of Monodisperse Ni Nanoparticles. *J. Phys. Chem. B* **2005**, *109* (25), 12257−12260.

(20) Hu, J.; Lu, Q.; Wu, C.; Liu, M.; Li, H.; Zhang, Y.; Yao, S. Synthesis of Fluorescent and Water-Dispersed Germanium Nanoparticles and Their Cellular Imaging Applications. *Langmuir* **2018**, *34* (30), 8932−8938.

(21) Muthuswamy, E.; Iskandar, A. S.; Amador, M. M.; Kauzlarich, S. M. Facile Synthesis of Germanium Nanoparticles with Size Control: Microwave versus Conventional Heating. *Chem. Mater.* **2013**, *25* (8), 1416−1422.

(22) Tabatabaei, K.; Holmes, A. L.; Newton, K. A.; Muthuswamy, E.; Sfadia, R.; Carter, S. A.; Kauzlarich, S. M. Halogen-Induced Crystallinity and Size Tuning of Microwave Synthesized Germanium Nanocrystals. *Chem. Mater.* **2019**, *31* (18), 7510−7521.

(23) Reid, W. E. Some Electrochemical Aspects of Germanium Dissolution. Simultaneous Chemical and Electrochemical Oxidation. *J. Phys. Chem.* **1965**, *69* (7), 2269−2277.

(24) Tabatabaei, K.; Sully, H. R.; Ju, Z.; Hellier, K.; Lu, H.; Perez, C. J.; Newton, K. A.; Brutchey, R. L.; Bridges, F.; Carter, S. A.; Kauzlarich, S. M. Structural Insights on Microwave-Synthesized Antimony-Doped Germanium Nanocrystals. *ACS Nano* **2021**, *15* (1), 1685−1700.
(25) Newton, K. A.; Ju, Z.; Tabatabaei, K.; Kauzlarich, S. M. Diorganyl Dichalcogenides as Surface Capping Ligands for Germanium Nanocrystals. *ACS Appl. Mater. Interfaces* **2020**, *39*, 995.
(26) Esteves, R. J. A.; Ho, M. Q.; Arachchige, I. U. Nanocrystalline Group IV Alloy Semiconductors: Synthesis and Characterization of $Ge_{1-x}Sn_x$ Quantum Dots for Tunable Bandgaps. *Chem. Mater.* **2015**, *27* (5), 1559−1568.
(27) Ruddy, D. A.; Erslev, P. T.; Habas, S. E.; Seabold, J. A.; Neale, N. R. Surface Chemistry Exchange of Alloyed Germanium Nanocrystals: A Pathway toward Conductive Group IV Nanocrystal Films. *J. Phys. Chem. Lett.* **2013**, *4* (3), 416−421.
(28) Tallapally, V.; Nakagawara, T. A.; Demchenko, D. O.; Özgür, Ü.; Arachchige, I. U. $Ge_{1-x}Sn_x$ Alloy Quantum Dots with Composition-Tunable Energy Gaps and near-Infrared Photoluminescence. *Nanoscale* **2018**, *10* (43), 20296−20305.
(29) Sully, H. R.; Tabatabaei, K.; Hellier, K.; Newton, K. A.; Ju, Z.; Knudson, L.; Zargar, S.; Wang, M.; Kauzlarich, S. M.; Bridges, F.; Carter, S. A. Characterizing Bismuth Doping of Colloidal Germanium Quantum Dots for Energy Conversion Applications. *ACS Appl. Nano Mater.* **2020**, *3* (6), 5410−5420.
(30) Bernard, A.; Zhang, K.; Larson, D.; Tabatabaei, K.; Kauzlarich, S. M. Solvent Effects on Growth, Crystallinity, and Surface Bonding of Ge Nanoparticles. *Inorg. Chem.* **2018**, *57* (9), 5299−5306.
(31) Scherrer, P. Determination of the Internal Structure and Size of Colloid Particles by X-Rays. *Göttinger Nachrichten Gesell* **1918**, *2*, 98−100.
(32) Kumar, K.; Chowdhury, A. Pushing the Limits of Analytical Characterization Tools: How Much Is Too Much? *Handb. Miniaturization Anal. Chem.* **2020**, 239−275.
(33) Matioszek, D.; Ojo, W. S.; Cornejo, A.; Katir, N.; El Ezzi, M.; Le Troedec, M.; Martinez, H.; Gornitzka, H.; Castel, A.; Nayral, C.; Delpech, F. From Rational Design of Organometallic Precursors to Optimized Synthesis of Core/Shell Ge/GeO_2 Nanoparticles. *Dalt. Trans.* **2015**, *44* (16), 7242−7250.
(34) Kwon, Y.; Kim, S. Indium Phosphide Magic-Sized Clusters: Chemistry and Applications. *NPG Asia Mater.* **2021**, *13* (1), 1−16.
(35) Smock, S. R.; Tabatabaei, K.; Williams, T. J.; Kauzlarich, S. M.; Brutchey, R. L. Surface Coordination Chemistry of Germanium Nanocrystals Synthesized by Microwave-Assisted Reduction in Oleylamine. *Nanoscale* **2020**, *12* (4), 2764−2772.
(36) Hellier, K. Understanding the Impact of Local Structure on Materials for Optoelectronic Applications. Ph.D. Thesis, University of California Santa Cruz, 2020. https://www.proquest.com/docview/2491206104?pq-origsite=gscholar&fromopenview=true (accessed Sep 25, 2021).
(37) Guyot-Sionnest, P.; Lhuillier, E.; Liu, H. A Mirage Study of CdSe Colloidal Quantum Dot Films, Urbach Tail, and Surface States. *J. Chem. Phys.* **2012**, *137* (15), 154704.
(38) Cody, G. D. Urbach Edge of Crystalline and Amorphous Silicon: A Personal Review. *J. Non. Cryst. Solids* **1992**, *141* (C), 3−15.
(39) Wang, B.; Wong, K. Y.; Yang, S.; Chen, T. Crystallinity and Defect State Engineering in Organo-Lead Halide Perovskite for High-Efficiency Solar Cells. *J. Mater. Chem. A* **2016**, *4* (10), 3806−3812.
(40) He, M.; Protesescu, L.; Caputo, R.; Krumeich, F.; Kovalenko, M. V. A General Synthesis Strategy for Monodisperse Metallic and Metalloid Nanoparticles (In, Ga, Bi, Sb, Zn, Cu, Sn, and Their Alloys) via in Situ Formed Metal Long-Chain Amides. *Chem. Mater.* **2015**, *27* (2), 635−647.
(41) Chen, M.; Feng, Y. G.; Wang, X.; Li, T. C.; Zhang, J. Y.; Qian, D. J. Silver Nanoparticles Capped by Oleylamine: Formation, Growth, and Self-Organization. *Langmuir* **2007**, *23* (10), 5296−5304.
(42) Pescara, B.; Mazzio, K. A.; Lips, K.; Raoux, S. Crystallinity and Size Control of Colloidal Germanium Nanoparticles from Organogermanium Halide Reagents. *Inorg. Chem.* **2019**, *58* (8), 4802−4811.
(43) Mourdikoudis, S.; Liz-Marzán, L. M. Oleylamine in Nanoparticle Synthesis. *Chem. Mater.* **2013**, *25* (9), 1465−1476.
(44) Nam, K. M.; Shim, J. H.; Ki, H.; Choi, S. Il; Lee, G.; Jang, J. K.; Jo, Y.; Jung, M. H.; Song, H.; Park, J. T. Single-Crystalline Hollow Face-Centered-Cubic Cobalt Nanoparticles from Solid Face-Centered-Cubic Cobalt Oxide Nanoparticles. *Angew. Chemie - Int. Ed.* **2008**, *47* (49), 9504−9508.
(45) Xue, D. J.; Wang, J. J.; Wang, Y. Q.; Xin, S.; Guo, Y. G.; Wan, L. J. Facile Synthesis of Germanium Nanocrystals and Their Application in Organic-Inorganic Hybrid Photodetectors. *Adv. Mater.* **2011**, *23* (32), 3704−3707.
(46) Hiramatsu, H.; Osterloh, F. E. A Simple Large-Scale Synthesis of Nearly Monodisperse Gold and Silver Nanoparticles with Adjustable Sizes and with Exchangeable Surfactants. *Chem. Mater.* **2004**, *16* (13), 2509−2511.
(47) Zhang, D.; Gill, L. A.; Cooks, R. G. Deamination of Protonated Amines to Yield Protonated Imines. *J. Am. Soc. Mass Spectrom.* **1998**, *9* (11), 1146−1157.
(48) Thomson, J. W.; Nagashima, K.; MacDonald, P. M.; Ozin, G. A. From Sulfur-Amine Solutions to Metal Sulfide Nanocrystals: Peering into the Oleylamine-Sulfur Black Box. *J. Am. Chem. Soc.* **2011**, *133* (13), 5036−5041.
(49) Park, J.; Kang, E.; Son, S. U.; Park, H. M.; Lee, M. K.; Kim, J.; Kim, K. W.; Noh, H. J.; Park, J. H.; Bae, C. J.; Park, J. G.; Hyeon, T. Monodisperse Nanoparticles of Ni and NiO: Synthesis, Characterization, Self-Assembled Superlattices, and Catalytic Applications in the Suzuki Coupling Reaction. *Adv. Mater.* **2005**, *17* (4), 429−434.
(50) Kura, H.; Takahashi, M.; Ogawa, T. Synthesis of Monodisperse Iron Nanoparticles with a High Saturation Magnetization Using an $Fe(CO)_x$-Oleylamine Reacted Precursor. *J. Phys. Chem. C* **2010**, *114* (13), 5835−5838.
(51) Johnson, O. H. Germanium and Its Inorganic Compounds. *Chem. Rev.* **1952**, *51* (3), 431−469.
(52) Johnson, W. C.; Sidwell, A. E. Nitrogen Compounds of Germanium. IV. The Action of Ammonia and Amines on Germanium Tetraiodide. *J. Am. Chem. Soc.* **1933**, *55* (5), 1884−1889.
(53) Thomas, J. S.; Southwood, W. W. Germanium. Part IX. The Action of Amines and of Certain Other Organic Bases on Germanium Tetrachloride. The Structure of Germanium Imide. *J. Chem. Soc.* **1931**, *0*, 2083−2097.
(54) Peng, Y.; Guo, J. D.; Ellis, B. D.; Zhu, Z.; Fettinger, J. C.; Nagase, S.; Power, P. P. Reaction of Hydrogen or Ammonia with Unsaturated Germanium or Tin Molecules under Ambient Conditions: Oxidative Addition versus Arene Elimination. *J. Am. Chem. Soc.* **2009**, *131* (44), 16272−16282.
(55) Gerung, H.; Bunge, S. D.; Boyle, T. J.; Brinker, C. J.; Han, S. M. Anhydrous Solution Synthesis of Germanium Nanocrystals from the Germanium(II) Precursor $Ge[N(SiMe_3)_2]_2$. *Chem. Commun.* **2005**, 1914−1916.
(56) Lee, H.; Yoon, D. E.; Koh, S.; Kang, M. S.; Lim, J.; Lee, D. C. Ligands as a Universal Molecular Toolkit in Synthesis and Assembly of Semiconductor Nanocrystals. *Chem. Sci.* **2020**, *11* (9), 2318−2329.

https://doi.org/10.1021/acsmaterialsau.1c00072
ACS Mater. Au 2022, 2, 330−342